Electric Power Systems Research 190 (2021) 106572

Contents lists available at ScienceDirect

Electric Power Systems Research

journal homepage: www.elsevier.com/locate/epsr

Protection strategy for fault detection in inverter-dominated low voltage AC microgrid

José Octávio Cesário Pereira Pinto*, Miguel Moreto

Department of Electrical and Electronics Engineering, Federal University of Santa Catarina, UFSC, Florianópolis, Brazil

ARTICLE INFO

Keywords:
Fault detection
Inverter-based distributed generation
Low voltage microgrids
Power systems protection
Renewable sources of energy

ABSTRACT

This paper presents a protection strategy based on active power flow direction, current magnitude and voltage sags to determine the existence of low impedance faults in inverter-dominated low voltage AC microgrids. Different fault situations are considered, concerning each element of the microgrid (line section, load, node and energy sources). Simulation is done in MATLAB/Simulink software. Microgrid was modelled based on CIGRE benchmark for network integration of renewable and distributed energy resources, considering the low voltage european distribution network characteristics. Inverter-based distributed generation units were modelled considering a control scheme composed by natural reference frame control and RMS current limiter. The results obtained from simulations indicate that the proposed strategy is able to protect the microgrid in any topology configuration or mode of operation, for all type of low impedance faults.

1. Introduction

One of the most challenging aspects of microgrids is its protection system, which plays a fundamental role in ensuring equipment's integrity and, consequently, in eletric shock protection. The presence of distributed generation (DG) and the possibility of operating either in grid-connected mode or in islanded mode leads the conventional protection devices to be inefficient. Furthermore, the fast expansion of the use of Renewable Energy Resources has lead a constant increase in Inverter-Based Distributed Generation (IBDGs) employment on microgrids. Studies have shown that the fault contribution of IBDG are dependent on its design, inverter control strategy and type of connection to the grid, fact that leads fault contribution current to be very particular to the employed IBDG characteristics. Moreover, IBDGs usually have its fault current contribution magnitude limited in 2 p.u., in order to protect its power electronic interface. Considering these aspects, fault detection becomes a very complex task in inverter-dominated microgrids.

Studies have corroborated the sighting that one of the main impediments associated to the microgrid's operation, regarding all its possible topological configuration, is its protection system. Since the traditional protective devices cannot provide complete safe operation to microgrids, islanded operation is usually not allowed by utilities and power distribution operators [1–4]. Therefore, the need of developing protective systems that are capable of working accurately for different topologies and types of faults has led researchers to investigate countless protective strategies and methods.

Several studies have been conducted to overcome the challenges of implementing a protection system for microgrids. Low voltage microgrid protection strategies found in the literature employ techniques and methods such as: harmonic distortion measurements [5], Wavelet transform [6], Clarke and Park transforms [7], methods based on differential protection [8], algorithms that recalculate short-circuit currents and relay adjustments according to changes in the microgrid topology [9], voltage sag detection [10], microgrid impedance methods [11] and artificial intelligence techniques [12–15]. The cited studies do not completely attend the aspects of interest of a protection scheme dedicated to a microgrid, such as the plug-and-play concept and the capabilty to adapt to real time operating conditions.

Thus, this work proposes a detection strategy to overcome the above-mentioned challenges by using simple-measurable parameters, such as active power flow direction and current and voltage magnitudes. These parameters are measured in strategic points of the microgrid. The proposed strategy does not relies on data centralization, accurate temporal synchronization or fixed-adjustments, and it is able to protect the microgrid in any topology configuration or mode of operation. The effectiveness of the proposed strategy is demonstrated by the simulation of faults in a microgrid modeled in MATLAB/Simulink.

* Corresponding author.
E-mail addresses: jocppa@outlook.com (J.O.C.P. Pinto), miguel.moreto@ufsc.br (M. Moreto).

https://doi.org/10.1016/j.epsr.2020.106572
Received 17 September 2019; Received in revised form 19 April 2020; Accepted 20 July 2020
Available online 05 August 2020
0378-7796/

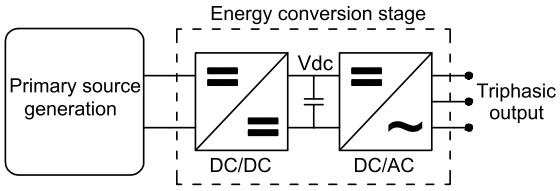

Fig. 1. Typical configuration of an IBDG unit.

2. Fault behaviour in inverter-based distributed generation units

An IBDG unit is typically composed of a primary source of generation and an energy conversion stage, as observed in Fig. 1. Microturbines, fuel cells, solar panels, batteries and wind generators are examples of technologies that can be used as a primary source in IBDG units. The energy conversion stage presented in Fig. 1 represents the most common configuration for this type of application, composed by a DC/DC converter, a link capacitor and a DC/AC converter (Voltage Source Inverter - VSI) [16]. The link capacitor is usually designed with high energy storage capacity in order to meet sudden changes in demand and afford the operational dynamics of the technology used as primary generation source. In these conditions, the link capacitor voltage tends to be constant during the operation of the presented IBDG configuration [17].

Thus, the IBDG configuration shown in Fig. 1 can be simplified to the model presented by Fig. 2, with constant voltage input *Vdc*. Therefore, the fault behaviour of an IBDG relies essentially on the DC/AC converter characteristics and its control strategies.

Studies have shown that the fault response of IBDGs are intrinsically related to its control strategy [3,18–20]. The control strategy used in an IBDG unit is defined according to its operational condition and the nature of its interaction with the microgrid. The strategies applied to IBDGs are commonly based on a multi-loop structure, composed of an Inner-Loop and an Outer-Loop control. Several methods can be used to achieve the purpose of these loops, and its determination relies on the IBDG adopted mode of control, that can be classified as grid-forming or grid-following. Fig. 3 shows numerous possible combinations that can be employed in an IBDG control strategy regarding its mode of operation and methods that can be used. The study presented in [21] discusses different aspects and possibilities of AC microgrids control strategies with IBDGs insertion.

From the standpoint of the microgrid protection, the endless possibilities of IBDGs control strategies bring on challenges to be overcome. Since it is not possible to predict the fault behaviour of an IBDG without knowing its employed control strategy, microgrid protection is one of the most challenging aspects to be implemented in real microgrids applications.

3. IBDG fault modelling

The IBDG model developed for the simulation was modelled considering the grid-following mode of control, aiming to afford microgrid islanded and grid-connected mode of operation. This was possible because the test microgrid model has a synchronous generator to ensure energy balance. Fig. 4 shows a typical control scheme used for IBDGs in grid-following mode.

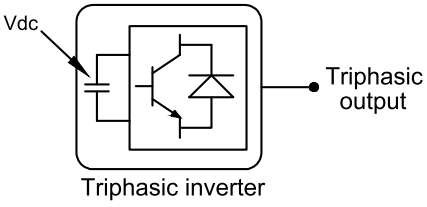

Fig. 2. Simplified IBDG model.

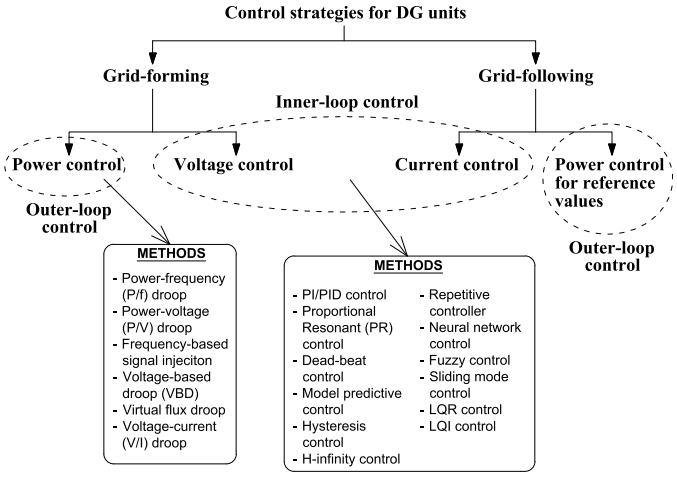

Fig. 3. IBDGs control strategies and possible methods [21].

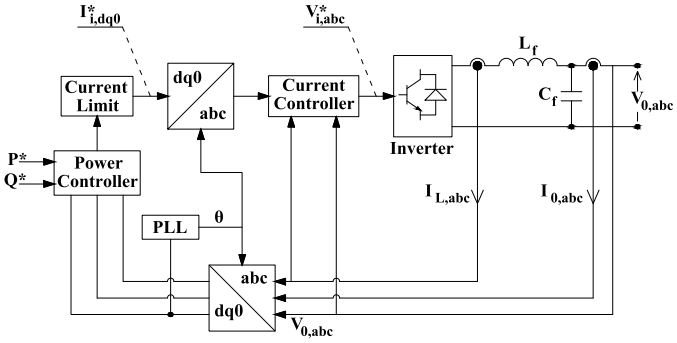

Fig. 4. Typical control scheme used for IBDGs in grid-following mode [3].

Note that the presented diagram is composed of distinct blocks, with different objectives, so that the desired control can be achieved. Each of these blocks has an extensive variety of internal methods that can be employed to perform its function. The blocks presented in the diagram are listed below:

- Current limiter: responsible for limiting the output current magnitude of the inverter.
- Current controller: responsible for controlling the current quality.
- Power controller: responsible for controlling the active and reactive power injection in the grid.
- PLL: responsible for obtaining the phase of the measured voltage at the IBDG connection point.
- dq0/abc: responsible for converting the reference frame of the measured parameters.

The wide variety of control strategies presented in Fig. 3, along with the operational characteristics presented in Fig. 4, elucidates the vast number of techniques and methods combinations that can be used to implement control scheme of IBDGs. Currently, there is no established norms or standardized design rules for development of IBDGs control strategies [21]. Consequently, IBDGs short-circuit contribution varies according to its technical characteristics. Therefore, fault detection in inverter-dominated microgrids becomes a complex issue.

Based on the studies presented in [18] and [3], the IBDG model used in this work was developed regarding three main characteristics:

- Use of Natural reference frame (NARF): allows independent control of each of the IBDG phase.
- Use of RMS current limiter: avoids current waveform output

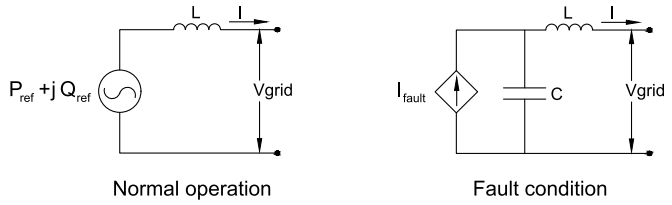

Fig. 5. IBDG model.

distortion when limiting the fault current contribution.

- Use of Proportional-Resonant(PR) Controller: enables the use of NARF and RMS current limiter.

Thus, the developed IBDG model can be represented by the diagram of Fig. 5. Therefore, during microgrid's normal operation, the IBDG model is controlled based on the voltage of its point of connection, in order to achieve the power supply referece. On the other hand, during the fault condition, the IBDG model operates as a current source, providing a maximum current magnitude value of 2 p.u. Similiar IBDG models are also proposed in 19,20,22,23,24

4. Microgrid test system

An inverter-dominated low-voltage AC microgrid was modelled based on technical parameters of European distribution grids. The development of the microgrid model was realized mostly based on the benchmark proposed in [4]. Fig. 6 illustrates the unifilar diagram of the proposed microgrid, which is composed of 9 residential/commercial loads (L1–L9), 7 inverter-based distributed generation units (IBDG1 - IBDG7) and 1 diesel generator (DGEN). The test system phases are balanced. The nodes of the microgrid are named by the letter "B" (e.g. B1, B2, B3...) while the line sections are named by the letters "DL" (e.g. DL1, DL2, DL3...). The small squares presented in the diagram of Fig. 6 represent the position of circuit breakers (CB) and measurement points.

Further details about the parameters used to build the model are presented in Appendix A.

4.1. Topology and operational restrictions

Two microgrid configurations were proposed in this work: microgrid operating in grid-connected mode of operation and microgrid operating in islanded mode of operation. Energy balance constraints are taken into consideration, since the total power load of the microgrid is 482 kVA, the total power supply capacity of IBDGs is 570 kVA and the DGEN has a maximum generation capacity of 350 kVA.

Aiming to attend ecological concerning and the above mentioned energy balance constraints, it is considered that the DGEN is active only during the islanded mode of operation. In this conditions, the DGEN plays a key role in the microgrid operation, since it is responsible for keeping the voltage and frequency stabilized. By contrast, during grid-connected mode of operation, the DGEN is considered to be inactive.

5. Proposed protection strategy

The proposed protection strategy considers four different fault situations, regarding the microgrid's elements: line section, load, node and DG. To perform the fault detection, strategic measurement points are determined along the proposed microgrid. The protection strategy is not affected by step-changes in the value of power and its sign forced by the operator or the control system.

5.1. Measured parameters

As can be seen in Fig. 6, line sections have measurements done in each of its extremity, whereas loads and DGs has one point of measurement each. These point of measurements are represented by the small square blocks of Fig. 6, and each block is composed of a circuit breaker and a meter.

Fig. 7 shows a branch of the modelled microgrid. Each measurement block is named according the element in which the block is situated and the adjacent node connection (e.g.: the measurement blocks presented

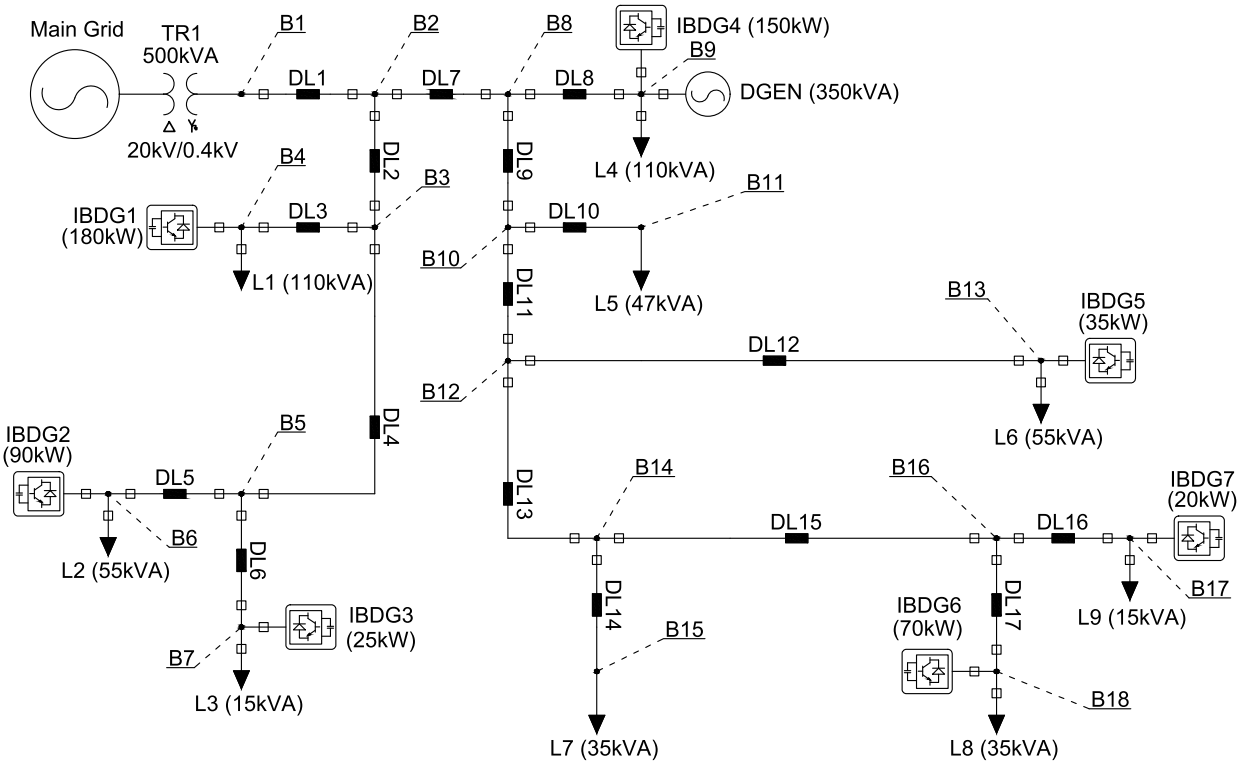

Fig. 6. Microgrid test system.

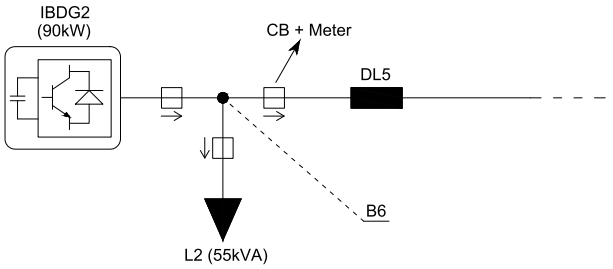

Fig. 7. Exemplification of the proposed power flow measurement convention.

in Fig. 7 are connected to node "B6", therefore these blocks names are "B6IBDG2", "B6DL5" and "B2L2").

The measurements are done with a sampling rate of 20 samples per electrical cycle. Each measurement device measures the following parameters per phase:

- Active power (magnitude and power flow direction).
- Voltage (RMS).
- Current (RMS).

Active power is calculated through (1) and a running average window of 1 electrical cycle is used for this calculation every 1 ms. Voltage and current phasors are estimated by MATLAB/Simulink.

$$P = \frac{|V|}{\sqrt{2}} \times \frac{|I|}{\sqrt{2}} \times \cos(\varphi) \tag{1}$$

where $\varphi = \angle V - \angle I$.

5.2. Fault detection strategy

A convention was stipulated to define the measured power flow direction by the system devices according to the element of the microgrid in which the meter is located. In case of an active element, the meter positive power flow is defined in the direction of the element to the node. In case of a passive element, the meter positive power flow is defined in direction of the node to the element. As can be observed in the diagram of Fig. 7, the meter positive power flow is represented by its respective arrow, and elucidates the stipulated convention.

The protection strategy is able to detect short-circuits according to the four different low impedance fault situations trough the following approaches:

1) *Line section:* the fault is detected by using active power flow direction per phase and voltage sags. In case of a fault, both extremities of the line section may experience incoming power flow, as can be seen in Fig. 8, where P1 and P2 are variables representing active power. Since the fault resistance (R_f) is low, a substantial voltage decrease is expected at the point of the fault incidence, thus causing the voltage sinking in the grid. Some microgrid's configurations may detect no power flow occurrence in one of the line section extremities. If there is no DG connected to the right side of the circuit extension in Fig. 8, P2 will decrease to values close to zero, fact that also allows the fault detection.
2) *DGs:* the fault is detected by using active power flow direction per phase. Fig. 9 shows an example of a DG fault occurrence. DGs are not expected to consume active power, therefore, regardless of the voltage sinking, a power flow inversion (P3) means the existence of a fault.
3) *Loads:* the fault is detected by using voltage sags and current magnitude increase per phase. These events are only present in the load under fault condition. An example of a load fault occurrence is presented in Fig. 10. Voltage sinking is caused by the low value of R_f. Considering the electrical grid configuration of Fig. 10, with two loads (L1 and L2) and one DG (IBDG), it is expected that the fault incidence at load L2 causes a substantial increase in current magnitude of I2 and also a noticeable decrease in current magnitude of I1. This behaviour is expected regardless of the number of loads in the microgrid.
4) *Nodes:* the fault is detected by using active power flow direction per phase and voltage sags. When the fault is located in a node, all elements connected to this node may experience active power flow direction towards the fault, as shown in Fig. 11.

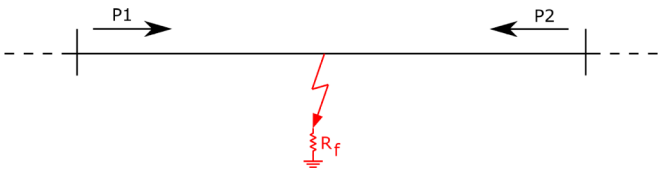

Fig. 8. Expected condition for a fault at line sections.

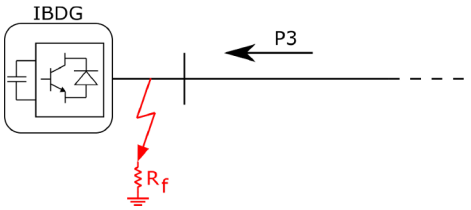

Fig. 9. Expected condition for a fault at DGs.

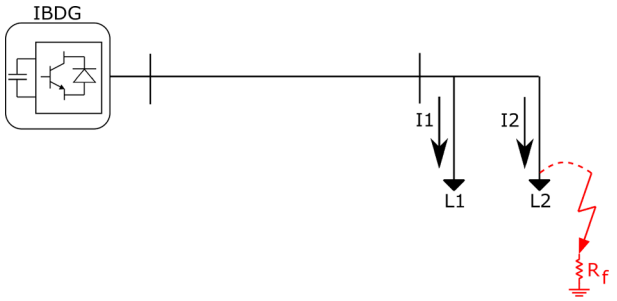

Fig. 10. Expected condition for a fault at loads.

During normal operation, the sum of active power in node B (P4, P5 and P6) should, ideally, be zero. In fault condition, changes in power flow direction may be detected, and the node active power sum may present an error out of tolerance. This event, along with the voltage sag detection, determines the existence of a fault.

6. Simulation and results

The proposed strategy is validated through the simulation of the microgrid model in MATLAB/Simulink. Different types of faults were

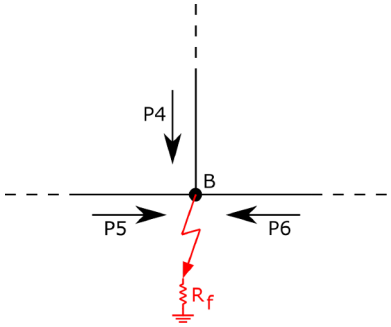

Fig. 11. Expected condition for a fault at nodes.

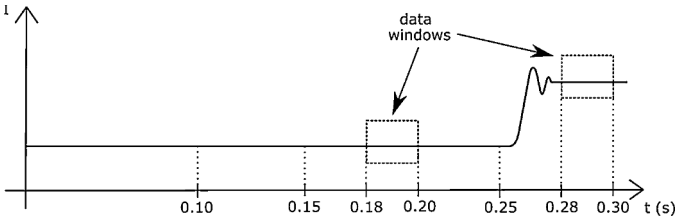

Fig. 12. Example of waveform and data windows.

simulated at different points of the microgrid, in order to attest the feasibility of the methodology. Simulations were performed with duration of 0.300 s. The short-circuit incidence occurs in time 0.250 s of the simulation. The used fault impedance is 0.001 Ω. Although only four case scenarios are presented in this paper, several other cases were simulated and the obtained results have also shown to be feasible.

Results are analyzed regarding two moments of the simulation: normal operation and contingency. Both are defined by a data window composed of 20 samples. The normal operation data window is measured between 0.180 s and 0.200 s while the contingency data window is measured between 0.280 s and 0.300 s of the simulation. An arithmetic mean value is obtained from each data window, resulting in one value for the normal operation moment and one value for the contingency moment to be analyzed. Since inverter-dominated microgrids provide fast response to short-circuits occurrence, the stipulated time interval between normal operation and contingency is considered conservative. Fig. 12 presents a waveform to exemplify the how results are analyzed.

Simulation of the four case scenarios are presented in this section, in order to attest the feasibility of each approach of proposed protection strategy. All the presented simulations were performed for both microgrid islanded and grid-connected mode of operation, and same results were obtained regarding the feasibility of the proposed strategy.

6.1. Fault at line section

For this case scenario, the microgrid is in isladed mode of operation and all IBDGs are active at 75% of their maximum power generation capacity. A three-phase fault (ABC-G) is applied at the extremity of line section DL17, close to the node B16. Voltage information obtained from the simulation is shown in Table 1. These values are obtained from the voltage measurement of each meter located in the microgrid. A brief analysis of the voltage levels corroborates the assumption of the severe voltage sinking in the microgrid within a fault occurrence. Fig. 13 shows a branch of the microgrid, in which the fault is located.

The convention adopted for the power flow measurement assures that a line section has always opposite direction of measurements at its extremities. Thus, under normal operation, the active power flow in a line section necessarily produces measurements with opposite signs in its meters. Table 2 shows active power flow values for the meters placed at both extremities of the line section under fault situation. The expected results are verified: in the normal operation the measures have opposite signs while in the contingency condition the measures have the same sign, indicating an inversion in the active power flow direction.

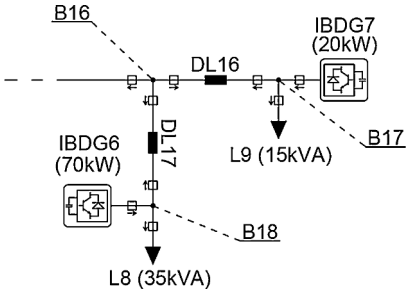

Fig. 13. Detailed view of the microgrid branch under fault condition.

Table 2
Active power per phase for case VI-A.

Meter	P_a (kW)		P_b (kW)		P_c (kW)	
	Norm.	Cont.	Norm.	Cont.	Norm.	Cont.
B16DL17	−5.953	**3.128**	−5.953	**3.048**	−5.953	**2.998**
B18DL17	5.958	**0.510**	5.958	**0.518**	5.958	**0.495**

6.2. Fault at load

For this case scenario, the microgrid is in isladed mode of operation and all IBDGs are active at 50% of their maximum power generation capacity, except for IBDG5 that is inactive. A two-phase fault (AB) is applied at load L6. Once again, voltage sinking can be observed in the faulted phases of the microgrid by analyzing the information presented in Table 3.

The feasibility of fault detection for the load approach is attested by analyzing the current values presented in Table 4, which represents the measurements of the meters placed at each load of the microgrid. By comparing the normal operation and the contingency conditions, it is noted that all meters has presented decreasing current behaviour, except for the meter B13L6 that is positioned in the load under fault condition. This circumstance, in combination with the voltage sinking attested by Table 3, corroborates the feasibility of the proposed approach.

6.3. Fault at node

For this case scenario, the microgrid is in grid-connected mode of operation and all IBDGs are active at 50% of their maximum power generation capacity. A single-phase fault (A-G) is applied at node B5. Voltage sinking can be attested for this scenario by analyzing the

Table 1
Voltage information for case VI-A.

Measured value	V_a (V)		V_b (V)		V_c (V)	
	Norm.	Cont.	Norm.	Cont.	Norm.	Cont.
Highest	233.7	147.8	233.7	148.0	233.7	147.9
Lowest	229.9	**1.9**	229.9	**1.8**	229.9	**1.8**
Mean	232.8	131.8	232.8	132.0	232.8	131.9

Table 3
Voltage information for case VI-B.

Measured value	V_a (V)		V_b (V)		V_c (V)	
	Norm.	Cont.	Norm.	Cont.	Norm.	Cont.
Highest	229.3	171.6	229.3	161.1	229.3	229.3
Lowest	222.1	**116.3**	222.1	**113.7**	222.1	**221.1**
Mean	225.1	158.1	225.1	151.5	225.1	225.1

Table 4
Current per phase for case VI-B.

Meter	I_a (A)		I_b (A)		I_c (A)	
	Norm.	Cont.	Norm.	Cont.	Norm.	Cont.
B4L1	155.0	108.9	155.0	107.0	155.0	155.0
B6L2	77.3	54.4	77.3	53.9	77.3	77.3
B7L3	21.1	14.8	21.1	14.7	21.1	21.1
B9L4	157.6	118.1	157.6	110.8	157.6	157.6
B13L6	76.4	**1502.3**	76.4	**1448.8**	76.4	76.4
B18L8	46.6	28.4	46.6	28.6	46.6	46.6
B17L9	21.0	12.8	21.0	12.9	21.0	21.0

Table 5
Voltage information for case VI-C.

Measured value	V_a (V)		V_b (V)		V_c (V)	
	Norm.	Cont.	Norm.	Cont.	Norm.	Cont.
Highest	229.5	103.8	229.4	288.9	229.4	338.2
Lowest	220.7	**22.4**	220.6	**271.6**	220.7	**322.1**
Mean	224.1	95.0	224.0	276.5	224.0	327.8

Table 6
Active power per phase for case VI-C.

Meter	P_a (kW)		P_b (kW)		P_c (kW)	
	Norm.	Cont.	Norm.	Cont.	Norm.	Cont.
B5DL4	−1.849	**−38.872**	−1.840	−14.499	−1.841	−26.154
B5DL5	1.507	**−5.271**	1.500	11.426	1.501	20.592
B5DL6	0.342	**−1.466**	0.340	3.072	0.340	5.561

Table 7
Active power per phase for case VI-D.

Meter	P_a (kW)		P_b (kW)		P_c (kW)	
	Norm.	Cont.	Norm.	Cont.	Norm.	Cont.
B4IBDG1	29.977	28.197	29.978	29.206	29.977	30.174
B6IBDG2	14.983	14.057	14.984	14.638	14.983	15.089
B7IBDG3	4.162	3.908	4.163	4.064	4.162	4.191
B9IBDG4	24.982	23.450	24.983	24.291	24.982	25.146
B13IBDG5	5.827	5.435	5.828	5.654	5.827	5.869
B18IBDG6	11.648	5.063	11.648	5.470	11.648	11.738
B17IBDG7	3.328	**−18.688**	3.328	1.765	3.328	3.354

information presented in Table 5.

Table 6 shows active power flow values for the meters placed at node B5 connected elements. It is possible to observe that, in the contingency condition, the sum of the power flow measured by the mentioned meters does not tend to be zero, therefore the feasibility of the proposed approach is attested.

6.4. Fault at IBDG

For this case scenario, the microgrid is in grid-connected mode of operation and all IBDGs are active at 50% of their maximum power generation capacity. A two-phase to ground fault (AB-G) is applied at IBDG7.

Since this approach is based only on the inversion of the active power flow, there is no need to verify the voltage sag occourrence in this scenario. Table 7 presents the power flow values for the meters that are positioned in all IBDGs of the microgrid. It can be noted that the power flow inversion is exclusively obtained by the meter B17IBGD7, which is located at the IBDG under fault condition. Therefore, the current approach of the proposed protection strategy has shown to be feasible.

7. Conclusion

The proposed strategy is validated through the simulation of a low voltage AC microgrid model, based on CIGRE benchmark parameters. The feasibility of the approaches for fault detection proposed within the protection strategy is proven by the presented results. The proposed strategy has shown to be effective for all types of low impedance faults situated at various points of the microgrid, since it is based on simple operating principle that does not rely exclusively on parameters magnitude or fixed adjustments. However, communication may be necessary for comparing measurements, fact that should not be a problem since communication features are considered intrinsic of microgrids. The protection strategy is able to detect faults regardless the microgrid topology, type or location of low impedance fault, factor that enhances the potential for applicability on real microgrid implementation. Results are presented for balanced operation and, based on the theoretical fundamentals used on the proposed methodology, it should also be effective for unbalanced operations. However, further studies for unbalanced microgrid conditions are under development to attest this supposition.

Declaration of Competing Interest

The authors declare that they have no known competing financial interests or personal relationships that could have appeared to influence the work reported in this paper.

Acknowledgments

This work was carried out with the support of CAPES, Coordination of Improvement of Higher Education Personnel - Brazil.

Appendix A. Microgrid Modeling

The data presented in this appendix refer to the parameters used in the microgrid modeling. The main grid was modeled as an ideal voltage source in series with an equivalent impedance, based on the parameters presented in Table 8.

The step-down transformer that provides the connection between medium and low voltage networks was modelled based on the parameters presented in Table 9.

The line sections were modelled as underground cables based on the parameters presented in Table 10, obtained from [4]. Due to the short line distances, capacitance of cable was disregarded. In Table 10, d_c is the conductor diameter, GMR is the geometric mean radius and a is the cables

Table 8
Medium voltage network equivalent parameters.

Nominal system voltage (kV)	Short-circuit power (MVA)	R/X ratio
20	100	1

Table 9
Transformer parameters.

Connection	Primary/secondary voltage (kV)	Impedance[a] (Ω)	Rated apparent power (kVA)	Transformer grounding (Ω)
3-phase, Dyn1	20/0.4	0.0032 + j0.0128	500	3

[a] Refers to the secondary side.

Table 10
Underground cable parameters.

Type of Conductor	Section (mm^2)	d_c (cm)	R_{ac} (Ω /km)	GMR (cm)	a (m)
NA2XY	240	1.75	0.162	0.634	0.90

Table 11
Synchronous generator parameters.

Rated apparent power (kVA)	Rated active power (kW)	Direct axis subtransient reactance X_d'' (%)	Phase resistance (mΩ)
350	280	14.0	12.5

depth. Inductance was calculated through (2), where GMD is the geometric average distance between the conductors [25].

$$L = 2{*}10^{-7}{*}\ln\left(\frac{GMD}{GMR}\right)[H/m] \quad (2)$$

Finally, the DGEN was considered as a three-phase synchronous generator, with 4 poles, in star-series connection, with nominal frequency and voltage of 50 Hz and 400 V respectively. Other parameters used to build this model are presented in Table 11.

References

[1] P. Dondi, D. Bayoumi, C. Haederli, D. Julian, M. Suter, Network integration of distributed power generation, J. Power Sources 106 (1) (2002) 1–9, https://doi.org/10.1016/S0378-7753(01)01031-X.

[2] J.C. Gomez, M.M. Morcos, Distributed generation: exploitation of islanding operation advantages, IEEE/PES Transmission and Distribution Conference and Exposition: Latin America, (2008), pp. 1–5, https://doi.org/10.1109/TDC-LA.2008.4641736.

[3] C.A. Plet, Fault Response of Inverter-Based Distributed Generation, (2012) Thesis.

[4] T.F.C. CIGRE, Benchmark Systems for Network Integration of Renewable and Distributed Energy Resources (2014).

[5] S.F. Zarei, M. Parniani, A comprehensive digital protection scheme for low-voltage microgrids with inverter-based and conventional distributed generations, IEEE Trans. Power Deliv. 32 (1) (2017) 441–452, https://doi.org/10.1109/TPWRD.2016.2566264.

[6] L. Zhou, G. Niu, Z.P. Qi, G.H. Gao, Y.G. Xu, Fault transient analysis in microgrid using discrete wavelet transform, 5th International Conference on Electric Utility Deregulation and Restructuring and Power Technologies (DRPT), (2015), pp. 1025–1029, https://doi.org/10.1109/DRPT.2015.7432381.

[7] H. Al-Nasseri, M.A. Redfern, F. Li, A voltage based protection for micro-grids containing power electronic converters, IEEE Power Engineering Society General Meeting, (2006), p. 7pp., https://doi.org/10.1109/PES.2006.1709423.

[8] M.P. Nthontho, S.P. Chowdhury, S. Winberg, S. Chowdhury, Protection of domestic solar photovoltaic based microgrid, 11th IET International Conference on Developments in Power Systems Protection (DPSP 2012), (2012), pp. 1–6, https://doi.org/10.1049/cp.2012.0137.

[9] K. Lai, M.S. Illindala, M.A. Haj-ahmed, Comprehensive protection strategy for an islanded microgrid using intelligent relays, IEEE Trans. Ind. Appl. 53 (1) (2017) 47–55, https://doi.org/10.1109/TIA.2016.2604203.

[10] M.A. Zamani, T.S. Sidhu, A. Yazdani, A protection strategy and microprocessor-based relay for low-voltage microgrids, IEEE Trans. Power Deliv. 26 (3) (2011) 1873–1883, https://doi.org/10.1109/TPWRD.2011.2120628.

[11] W. Huang, N. Tai, K. Li, X. Zheng, S. Chen, Protection scheme for active distribution networks using positive-sequence components, 2015 IEEE Power Energy Society General Meeting, (2015), pp. 1–5, https://doi.org/10.1109/PESGM.2015.7286368.

[12] D.P. Mishra, S.R. Samantaray, G. Joos, A combined wavelet and data-mining based intelligent protection scheme for microgrid, IEEE Trans. Smart Grid 7 (5) (2016) 2295–2304, https://doi.org/10.1109/TSG.2015.2487501.

[13] J.J.Q. Yu, Y. Hou, A.Y.S. Lam, V.O.K. Li, Intelligent fault detection scheme for microgrids with wavelet-based deep neural networks, IEEE Trans. Smart Grid PP (99) (2017) 1, https://doi.org/10.1109/TSG.2017.2776310.

[14] M.H. Cintuglu, T. Ma, O.A. Mohammed, Protection of autonomous microgrids using agent-based distributed communication, IEEE Trans. Power Deliv. 32 (1) (2017) 351–360, https://doi.org/10.1109/TPWRD.2016.2551368.

[15] H.F. Habib, T. Youssef, M.H. Cintuglu, O.A. Mohammed, Multi-agent-based technique for fault location, isolation, and service restoration, IEEE Trans. Ind. Appl. 53 (3) (2017) 1841–1851, https://doi.org/10.1109/TIA.2017.2671427.

[16] F. Katiraei, R. Iravani, N. Hatziargyriou, A. Dimeas, Microgrids management, IEEE Power Energy Mag. 6 (3) (2008) 54–65, https://doi.org/10.1109/MPE.2008.918702.

[17] R.H. Lasseter, P. Piagi, Control and Design of Microgrid Components, Report, University of Wisconsin, 2006.

[18] M. Brucoli, Fault Behaviour and Fault Detection in Islanded Inverter-Only Microgrids, (2008) Thesis.

[19] C. A. Plet, M. Brucoli, J. D. F. McDonald and T. C. Green, "Fault models of inverter-interfaced distributed generators: Experimental verification and application to fault analysis," 2011 IEEE Power and Energy Society General Meeting, Detroit, MI, USA, 2011, pp. 1-8, doi: 10.1109/PES.2011.6039183.

[20] T. Dao Van, S. Chaitusaney, Impacts of inverter-based distributed generation control modes on short-circuit currents in distribution systems, 7th IEEE Conference on Industrial Electronics and Applications (ICIEA), (2012), pp. 1645–1650, https://doi.org/10.1109/ICIEA.2012.6360989.

[21] M. Hossain, H. Pota, W. Issa, Overview of AC microgrid controls with inverter-interfaced generations, Energies 10 (9) (2017) 1300.

[22] M. Brucoli, T.C. Green, J.D.F. McDonald, Modelling and analysis of fault behaviour of inverter microgrids to aid future fault detection, IEEE International Conference on System of Systems Engineering, (2007), pp. 1–6, https://doi.org/10.1109/SYSOSE.2007.4304253.

[23] C.A. Plet, M. Graovac, T.C. Green, R. Iravani, Fault response of grid-connected inverter dominated networks, IEEE PES General Meeting, (2010), pp. 1–8, https://doi.org/10.1109/PES.2010.5589981.

[24] T. Dao, S. Chaitusaney, Fault current calculation in system with inverter-based distributed generation with consideration of fault ride through requirement, volume 2, 2013.

[25] M. Grobler, Determining Transmission Line Parameters From Time-Stamped Data, (2007) Thesis.